ACS Pharmacology & Translational Science

Article

Cite This: ACS Pharmacol. Transl. Sci. 2019, 2, 114−121

pubs.acs.org/ptsci

Calcitonin-Receptor-Like Receptor Signaling Governs Intestinal Lymphatic Innervation and Lipid Uptake

Reema B. Davis, Shengli Ding, Natalie R. Nielsen, John B. Pawlak, Elizabeth S. Blakeney, and Kathleen M. Caron*

Department of Cell Biology and Physiology, University of North Carolina Chapel Hill, 111 Mason Farm Road, 6312B Medical Biomolecular Research Building, CB#7545, Chapel Hill, North Carolina 27599-7545, United States

ABSTRACT: The absorption of dietary fat requires complex neuroendocrine-mediated regulation of chylomicron trafficking through enterocytes and intestinal lymphatic vessels. Calcitonin-receptor-like receptor (*Calcrl*) is a G protein-coupled receptor that can bind either a lymphangiogenic ligand adrenomedullin, with coreceptor RAMP2, or the neuropeptide CGRP, with coreceptor RAMP1. The extent to which this common GPCR controls lipid absorption via lymphatics or enteric innervation remains unclear. We used conditional and inducible genetic deletion of *Calcrl* in lymphatics to elucidate the pathophysiological consequences of this receptor pathway under conditions of high-fat diet. Inefficient absorption of dietary fat coupled with altered lymphatic endothelial junctions in $Calcrl^{fl/fl}$/*Prox1-CreER*^{T2} mice results in excessive, transcellular lipid accumulation and abnormal enterocyte chylomicron processing and failure to gain weight. Interestingly, $Calcrl^{fl/fl}$/*Prox1-CreER*^{T2} animals show reduced and disorganized mucosal and submucosal innervation. Consistently, mice with genetic loss of the CGRP coreceptor RAMP1 also displayed mucosal and submucosal innervation deficits, substantiating the CGRP-biased function of *Calcrl* in the neurolymphocrine axis. Thus, the common *Calcrl* receptor is a critical regulator of lipid absorption through its cell-specific functions in neurolymphocrine crosstalk.

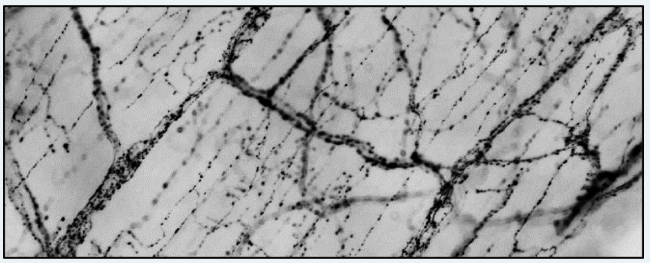

KEYWORDS: *lacteal, lipid absorption, CLR, CGRP, neurolymphocrine axis*

INTRODUCTION

Dietary fat absorption is a complex process and primarily occurs through specialized lymphatic vessels called lacteals that are present inside each intestinal villus. Lipid uptake requires a regulated crosstalk between intestinal lacteals, epithelium, enteroendocrine cells, and the enteric nervous system. In addition, nutrient sensing performed by sensory nerves balances intracellular metabolism, obesity, and behavior of food intake.[1] Most studies explore these systems in isolation; therefore, the exact nature of their interaction to promote fat absorption or dysregulation of the process in disease conditions is unclear.

Intestinal lacteals are central to dietary lipid uptake and their structure and function is largely governed by Notch, VEGF, and adrenomedullin signaling.[2−4] Lipid-rich lymph is propelled through paracellular fenestrated lymphatic endothelial junctions and by transcellular vesicular transport into the lacteal lumen.[5,6] Adrenomedullin (AM) can reorganize ZO-1 and VE-cadherin at the lymphatic endothelial cell (LEC) junctions resulting in dramatic changes in pathophysiology of mice lacking the key AM receptor calcitonin-receptor-like receptor (gene: *Calcrl*, protein: CLR) from their lymphatic vessels and enteroendocrine cells.[4,7] The ligand-binding affinity of CLR is determined by its interaction with receptor activity modifying protein (RAMPs). Upon heterodimerzing with RAMP2, CLR binds AM.[8] Recent evidence shows that AM treatment of LEC in vitro increases their transedothelial electric resistance altering albumin transport.[6] In addition to the widely accepted paracellular transport, transcellular vesicular transport mechanisms govern interstitial albumin uptake by dermal lymphatic vessels.[6] However, the extent to which the paracellular and transcellular pathways function in parallel in the intestinal lacteals thereby regulating dietary fat absorption under basal and disease conditions remains unknown.

Lipid uptake is also governed by the nerve-induced contractility of the smooth muscle cage surrounding the intestinal lacteals.[9] In addition to regulating intestinal smooth muscle contraction, sensory CGRP-releasing nerves connect with lacteals, and are thereby predicted to have mechanoreceptive functions.[1,10] CLR heterodimerizes with coreceptor RAMP1 to preferentially bind CGRP.[8,11] Moreover the epithelial lining of the gut comprises 1% enteroendocrine cells (EEC) responsible for secreting hormones such as ghrelin, PYY, GLP-1 and 2, and CCK, which are in direct contact with the enteric nerves engaging in afferent synaptic transmission through hormones and efferent neurotransmission through postsynaptic proteins.[12−14] However, the precise role of the CLR signaling axis in mediating lacteal and intestinal innervation is undetermined.

In this study, we examined the crosstalk between the lymphatic endothelium and the enteric nervous system in maintaining lipid homeostasis in the gut. We used $Calcrl^{fl/fl}$/*Prox1-CreER*^{T2} mice

Received: December 21, 2018
Published: January 29, 2019

DOI: 10.1021/acsptsci.8b00061
ACS Pharmacol. Transl. Sci. 2019, 2, 114−121

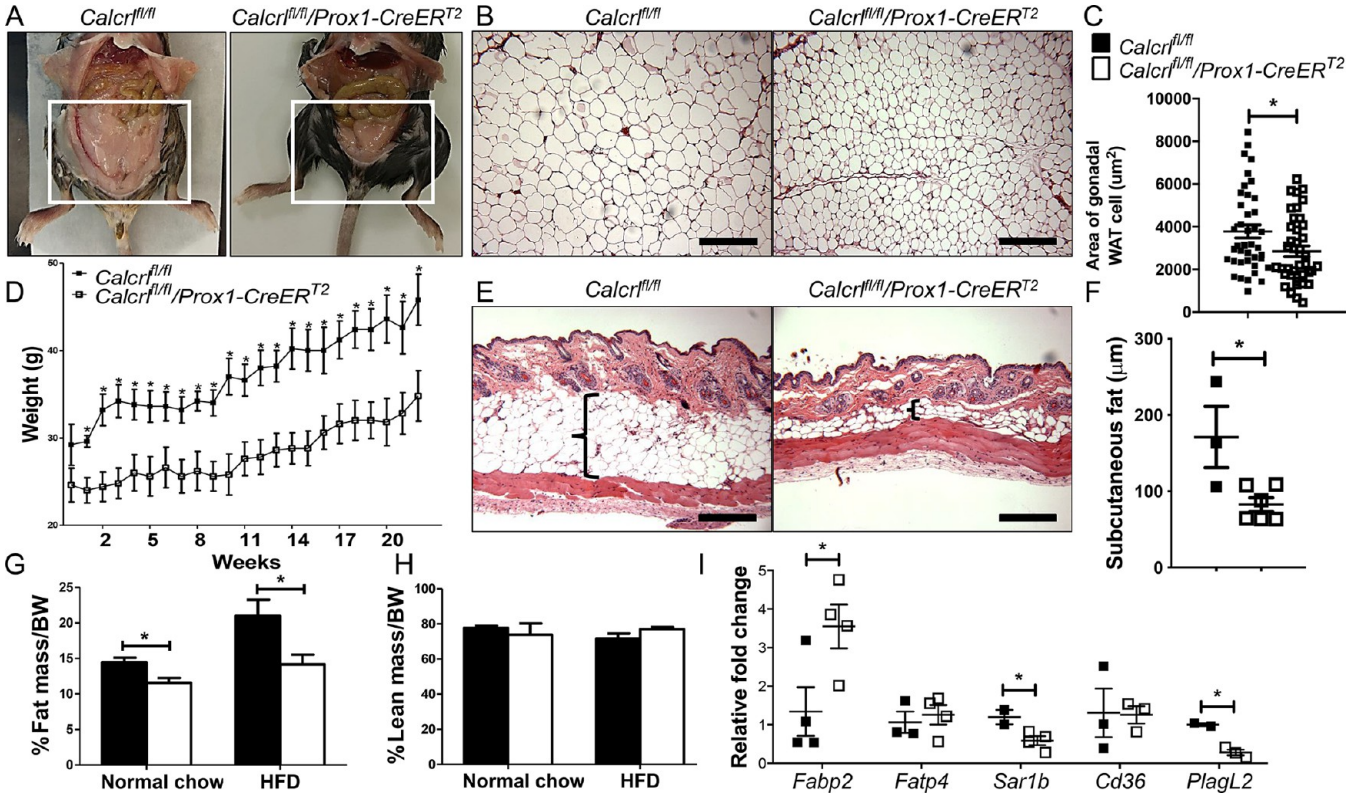

Figure 1. Loss of *Calcrl* severely attenuates body fat accumulation. (A) Gross images of *Calcrl*$^{fl/fl}$ and *Calcrl*$^{fl/fl}$/*Prox1-CreER*^{T2} animals after 22 weeks of HFD. Boxed regions highlight reduced gonadal fat. N = 16 animals per genotype. (B, C) Representative H&E stained images of gonadal white adipose tissue (WAT) from *Calcrl*$^{fl/fl}$ and *Calcrl*$^{fl/fl}$/*Prox1-CreER*^{T2} animals. Quantification of gonadal WAT cell area. Data are represented as mean ± SEM with significance determined by Student's t test: *, $P < 0.05$. N = 8 animals per genotype; the area of 10 cells/animal across the entire field of view was calculated. Scale bars: 500 μm. (D) Weight gain of *Calcrl*$^{fl/fl}$ and *Calcrl*$^{fl/fl}$/*Prox1-CreER*^{T2} animals over long-term HFD with significance determined by Student's t test: *, $P < 0.05$. N = 5 animals per genotype. (E, F) Representative H&E stained skin sections with brackets highlighting the subcutaneous fat layer of *Calcrl*$^{fl/fl}$ and *Calcrl*$^{fl/fl}$/*Prox1-CreER*^{T2} animals. Quantification of subcutaneous adipose layer width of *Calcrl*$^{fl/fl}$ and *Calcrl*$^{fl/fl}$/*Prox1-CreER*^{T2} animals. Data are represented as mean ± SEM with significance determined by Student's t test: *, $P < 0.05$. N = 6 animals per genotype. Scale bars: 500 μm. (G, H) MRI scans showing fat mass and lean mass of tamoxifen-treated *Calcrl*$^{fl/fl}$ and *Calcrl*$^{fl/fl}$/*Prox1-CreER*^{T2} animals. Quantitative data are represented as % mass over body weight (BW) ± SEM with significance determined by 2-tailed, type 2 Student's t test: *, $P < 0.05$. N = 4 *Calcrl*$^{fl/fl}$ and 9 *Calcrl*$^{fl/fl}$/*Prox1-CreER*^{T2}. (I) Relative expression of lipid transporters in tamoxifen-treated *Calcrl*$^{fl/fl}$ and *Calcrl*$^{fl/fl}$/*Prox1-CreER*^{T2} whole duodenum. *Gapdh* and *Rpl19* were used as housekeeping controls. Quantitative data are represented as % mass over body weight (BW) ± SEM with significance determined by 2-tailed, type 2 Student's t test: *, $P < 0.05$. N = 4 animals per genotype.

in which tamoxifen treatment causes the inducible excision of the *Calcrl* gene under the control of the *Prox1-CreER*^{T2} transgene in lymphatic endothelial cells, liver hepatocytes, retinal cells, and some cardiomyocytes. We demonstrate that genetic depletion of *Calcrl* from the lymphatic vessels obstructs lipid trafficking through the endothelium and alters the patterning of mucosal and submucosal nerves.

MATERIAL AND METHODS

Animals and Procedures. *Calcrl*$^{fl/fl}$ and *Calcrl*$^{fl/fl}$/*Prox1-CreER*^{T2} mice were injected with Tamoxifen (Sigma-Aldrich T5648) to induce *Calcrl* deletion.[4] The presence of wildtype, floxed, *Prox1-CreER*^{T2}, and excised alleles were detected by genotyping using primers 5′-GCGGAGCATATTCAATCACAAG-3′ and 5′-GAAATGTGCTGTATGTTCAAGC-3′, 5′-GCGGAGCATATTCAATCACAAG-3′ and 5′-GACGAGTTCTTCTGAGGGGA-3′, 5′-CGAGCTCTTTCTCTCTACAGTTCAACA-3′ and 5′-GGCCAGTAACGTTAGGGAGAGG-3′, 5′-GCGGAGCATATTCAATCACAAG-3′ and 5′-GAATAAGTTGAGCTGGGCAG-3′, respectively. *Ramp1*$^{-/-}$ and wildtype allele were genotyped using 5′-TCATGGGGACCTTTAGGTAAGC-3′ and 5′ ACAGCAATCCTTCTACCTCAACAC-3′.[15]

Mice were provided a high-fat diet (HFD) for either 10 or up to 22 weeks receiving 42% kcal from fat (TD.88137). Body weights, food, and water consumption were measured for the entire duration. At the end of the study the animals were housed individually in metabolic cages to harvest stool, urine, and monitor individual food and water consumption per animal per genotype. BODIPY-FL C_{16} (ThermoFisher Scientific D3821) was gavaged at 2 μg/g body weight after overnight fasting followed by 3 h incubation.

The number of animals used in each experiment is provided in the figure captions. Histological images reflect representative phenotypes observed using a minimum of 3 animals per genotype, with multiple areas of tissue evaluated. Scoring and image analysis was performed while blinded to the genotypes and/or treatment conditions. Animal procedures were approved by the University of North Carolina Chapel Hill's Institutional Animal Care and Use Committee and all attempts were made to minimize pain and distress.

Hepatic Triglyceride Production Rate. To calculate the hepatic triglyceride production rate, a nonionic detergent, Triton W-1339 (Sigma-Aldrich T0307−5G; 12.5 mg/100 μL PBS/mouse), was administered intraperitoneally followed by

DOI: 10.1021/acsptsci.8b00061
ACS Pharmacol. Transl. Sci. 2019, 2, 114−121

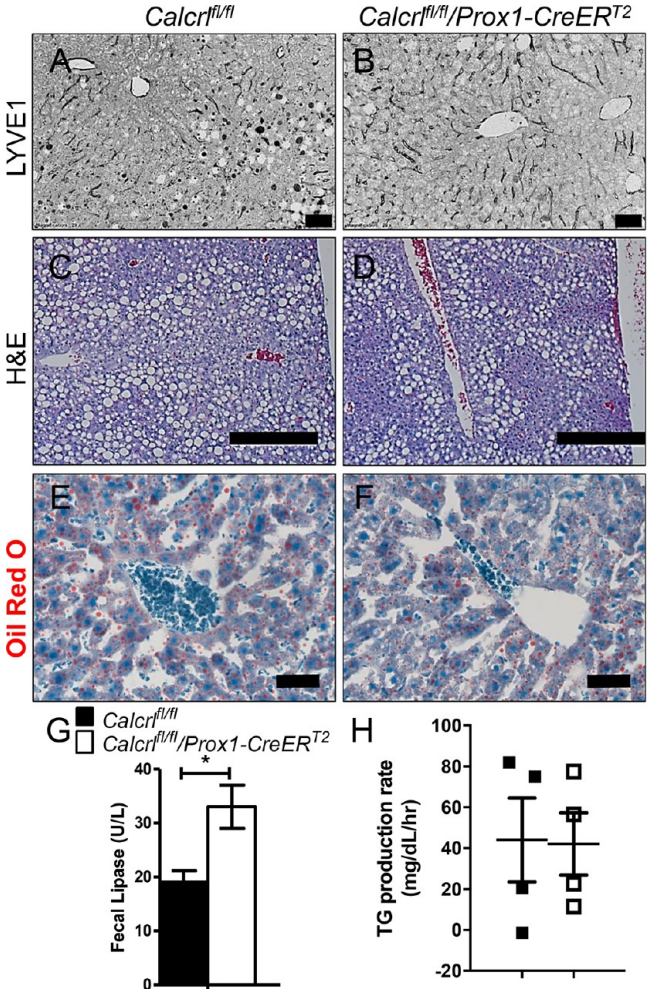

Figure 2. Dilated liver lymphatics with reduced lipid accumulation. (A, B) Representative LYVE1 stained images of liver from *Calcrl*$^{fl/fl}$ and *Calcrl*$^{fl/fl}$*/Prox1-CreER*^{T2} animals. Scale bars: 50 μm. $N = 8$ animals per genotype. (C, D) Representative H&E stained images of liver from *Calcrl*$^{fl/fl}$ and *Calcrl*$^{fl/fl}$*/Prox1-CreER*^{T2} animals. Scale bars: 400 μm. $N = 6$ animals per genotype. (E, F) Representative Oil red O stained images of liver from *Calcrl*$^{fl/fl}$ and *Calcrl*$^{fl/fl}$*/Prox1-CreER*^{T2} animals. Scale bars: 50 μm. $N = 4$ animals per genotype. (G) Relative levels of fecal lipase in *Calcrl*$^{fl/fl}$ and *Calcrl*$^{fl/fl}$*/Prox1-CreER*^{T2} animals. Data are represented as mean ± SEM with significance determined by Student's *t* test: *, $P < 0.05$. $N = 4$ animals per genotype. (H) Relative levels of plasma triglyceride levels (TG) data are represented triglyceride production rate ± SEM with significance determined by 2-tailed, type 2 Student's *t* test: *, $P < 0.05$. $N = 4$ animals per genotype.

measuring plasma triglyceride levels over 3 h.[16] The triglyceride production rate was calculated as the difference over 3 h following triton injection.

Plasma Lipid and Fecal Lipase Measurements. Blood was collected from cardiac puncture into EDTA coated-tubes (Milian 022379224). Plasma triglyceride levels were assayed by the Animal Clinical Chemistry and Gene Expression Lab at UNC.

MRI Analysis. Magnetic resonance imaging to quantify body fat, lean mass, and water content was performed by UNC's animal metabolism phenotyping core.

RNA and Quantitative RT-PCR. Whole duodenal tissue was collected in RNAlater (Ambion AM7021). TRIzol reagent (Ambion 15596026) was used for RNA extraction from tissue followed by DNase (Promega M6101) treatment. cDNA was prepared using M-MLV reverse transcriptase (Invitrogen, 28025−013). Quantitative RT-PCR was done on a StepOnePlus (ABI) using Taqman Mastermix (Applied Biosystems 4369016). Sox9 high and unsorted cells obtained from untreated intestines were also used for quantitative RT-PCR.[17] Mouse gene expression was assessed with single-tube assays: *Fabp2* (Mm00433188_m1), *Fatp4* (Mm01327405_m1), *Sar1b* (Mm00508430_m1), *Plagl2* (Mm01263610_m1), *Cd36* (Mm00432403_m1), *Rpl19* (Mm02601633_m1), *Calcrl* (Mm00516986_m1), *CGRP* (Mm00801463_g1), *Ramp1* (Mm00489796_m1), *Ramp2* (Mm00490256_g1), *Prox1* (Mm00435969_m1), and *Gapdh* (Mm99999915_g1). Comparative $\Delta\Delta C_T$ analysis for relative gene expression was normalized to housekeeping controls *Rpl19* or *Gapdh*.

Immunohistochemistry and Immunofluorescence. Small intestinal duodenum or jejunum cleaned with cold PBS and either scraped or fixed whole in 4% PFA or 10% zinc formalin (Protocol 313−095) overnight. Whole-mount staining was done using a slightly modified previously published protocol.[4,18] Briefly, 1 cm pieces of fixed duodenum or jejunum were passed through a glycerol and sucrose gradient and blocked in donkey serum, sodium azide, and BSA mix. Paraffin and cryosections were rehydrated, permeabilized using 1% Triton X-100 in PBS for 20 min, and then blocked in 5% NDS. Whole-mount or tissue sections were then incubated in primary antibodies including rabbit anti-LYVE-1 (1:200, Fitzgerald 70R-LR005), mouse anti-smooth muscle actin (1:200, Sigma-Aldrich A4700), Syrian hamster anti-podoplanin (1:200, Developmental studies hybridoma bank 8.1.1), rat anti-PECAM-1 (1:100, BD Pharmingen 550274), or rabbit anti-tyrosine hydroxylase (1:100, Novus Biologicals NB300−109) for 3 days. Intestines were washed, and incubated for 48 h in secondary antibodies, including a combination of donkey anti-rat IgG Cy3 (1:200, Jackson ImmunoResearch 712−165−150), or donkey anti-rabbit Cy3 or Cy5 (1:200, Jackson ImmunoResearch 711−225−152, 711−175−152), or goat anti-syrian hamster Cy3 (1:200, Jackson ImmunoResearch 307−165−003), and bisbenzimide H 33258 Hoechst (Sigma B1155) at 1:250. For antibodies requiring antigen retrieval, slides were boiled for 20 min in 10 mM citrate buffer using a microwave. The whole-mount tissues and sections were mounted in Prolong gold (Life technologies P36934). Hematoxylin and eosin and Oil red O staining were performed by the UNC Histology Research Core Facility.

Image Acquisition. H&E and Oil red O slides were imaged using a Leitz Dialux 20 with QImaging Micropublisher 5.0 RTV color CCD camera. Fluorescence IHC images were acquired either on a Nikon E800 fluorescence microscope with a Hammamatsu Orca CCD camera with Metamorph software (Molecular Devices Corp.) or a Zeiss 880 confocal with Airyscan superresolution sensor. Whole-mount fluorescent stained duodenum or jejunum was imaged using an Olympus IX-81 inverted fluorescent microscope equipped with a QImaging Retiga 4000R camera at 4× magnification. Images were deconvoluted and pseudocolored using Metamorph, Olympus cellSens, or ImageJ. Whole-mount entire small intestines were imaged using a Nikon 5200 DSLR camera. For ultramicroscopy studies, tissue was fixed in glutaraldehyde/paraformaldehyde. Transmission electron microscopy images were acquired on a Zeiss EM 910 microscope.

Statistical Analysis. All experiments were performed 3 or more times, and data is represented as a mean with SEM. Significance was either by determined by Student's *t* test (tail = 2,

DOI: 10.1021/acsptsci.8b00061
ACS Pharmacol. Transl. Sci. 2019, 2, 114−121

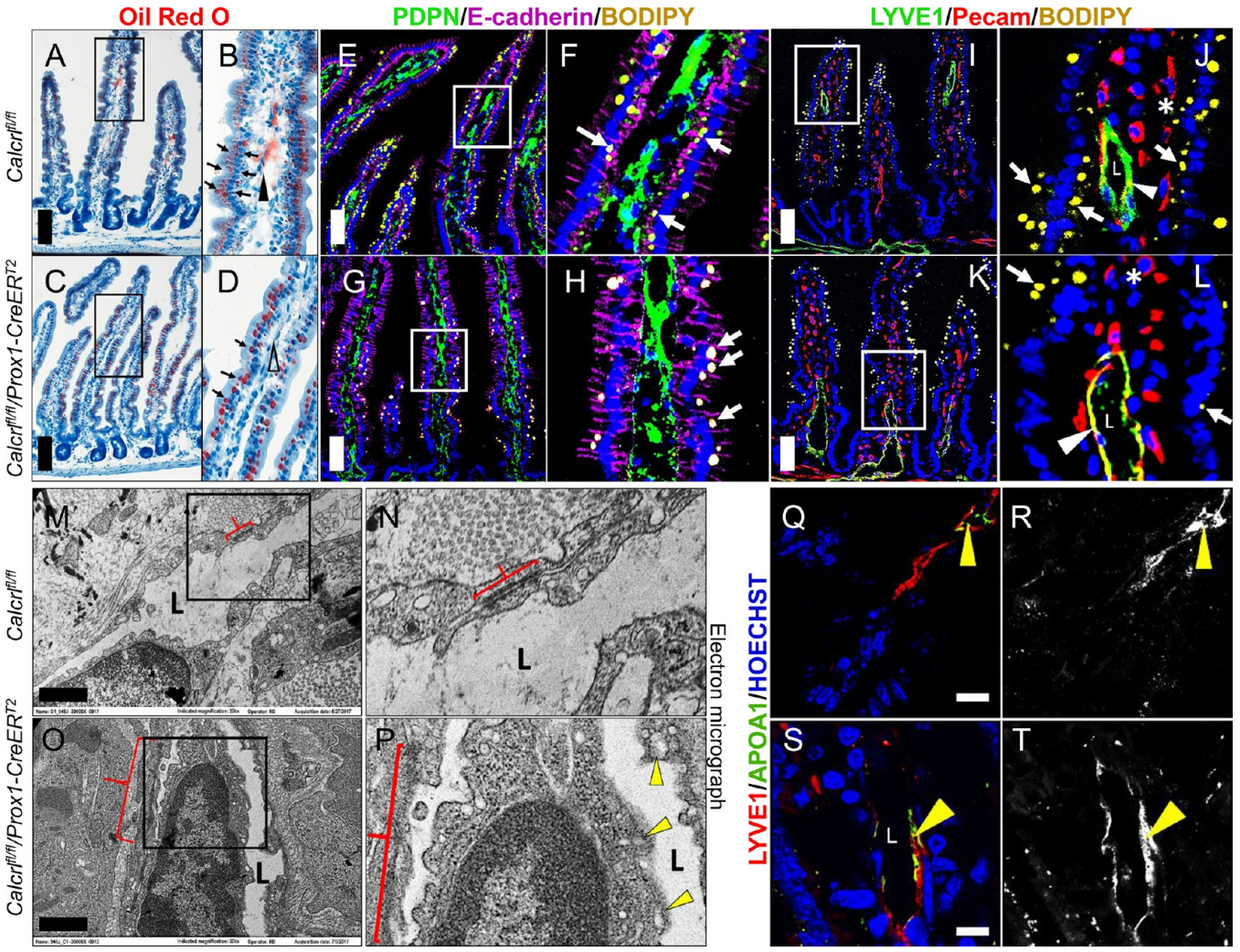

Figure 3. Dysregulation of lipid trafficking upon *Calcrl* depletion. (A−D) Representative oil red O stained sections of tamoxifen-treated *Calcrl*$^{fl/fl}$ and *Calcrl*$^{fl/fl}$/*Prox1-CreER*^{T2} animals after HFD challenge. Arrows highlight lipid deposits in enterocytes, and arrowheads mark lipid at the center of villi. Boxed regions are displayed as digitally zoomed insets on the right of each image. (E−H) Representative fluorescent images of Podoplanin and E-cadherin stained sections of tamoxifen *Calcrl*$^{fl/fl}$ and *Calcrl*$^{fl/fl}$/*Prox1-CreER*^{T2} animals after BODIPY gavage. Arrows indicate BODIPY droplets. Boxed regions are displayed as digitally zoomed insets on the right of each image. (I−L) Representative fluorescent images of LYVE1 and PECAM-stained sections of tamoxifen *Calcrl*$^{fl/fl}$ and *Calcrl*$^{fl/fl}$/*Prox1-CreER*^{T2} animals after BODIPY gavage. Arrows indicate BODIPY droplets, arrowheads highlight BODIPY accumulation within LECs, asterisk shows PECAM-labeled blood vessels, and "L" marks the lacteal lumen. Boxed regions are displayed as digitally zoomed insets on the right of each image. (M−P) Representative transmission electron microscopy images of tamoxifen *Calcrl*$^{fl/fl}$ and *Calcrl*$^{fl/fl}$/*Prox1-CreER*^{T2} lacteals after HFD challenge. Arrowheads indicate lipid droplets, red brackets highlight adherens junctions, and "L" marks the lacteal lumen. Boxed regions are displayed as digitally zoomed insets on the right of each image. (Q−T) Representative fluorescent images of LYVE1 and APOA1 stained sections of tamoxifen *Calcrl*$^{fl/fl}$ and *Calcrl*$^{fl/fl}$/*Prox1-CreER*^{T2} animals after BODIPY gavage. Arrowheads highlight APOA1 chylomicron accumulation within LECs or within the lacteal lumen. For all panels in Figure 3: $N = 4-6$ animals per genotype. Scale bars: 100 μm in (A, C); 50 μm in (E, G, I, K); 1 μm in (M, O).

type = 2) or one-way ANOVA with Tukey's Multiple comparison test with *, $p < 0.05$. Kaplan−Meier test was done to test survival.

RESULTS

***Calcrl* Deletion in Lymphatics Limits Weight Gain after a 22 week HFD Challenge.** To determine the full extent to which the depletion of *Calcrl* from the lymphatic endothelium and the enteroendocrine cells alters body weight equilibrium, we examined the fat composition of tamoxifen-treated *Calcrl*$^{fl/fl}$ and *Calcrl*$^{fl/fl}$/*Prox1-CreER*^{T2} animals after 22 weeks of HFD. Although both the groups ate and drank similar amounts of food (∼4g/day) and water (∼3−4 mL/day), the gonadal white adipose tissue (WAT) of *Calcrl*$^{fl/fl}$/*Prox1-CreER*^{T2} appeared grossly smaller (∼1/3rd of control), with reduced weight and cell area (Figure 1A−C). Weight gain of *Calcrl*$^{fl/fl}$/*Prox1-CreER*^{T2} animals remained limited over 22 weeks of HFD (Figure 1D). Likewise, their subcutaneous fat layer was significantly reduced (Figure 1E,F). MRI scanning revealed similar lean mass and water composition (data not shown) for the two groups but significantly diminished fat mass in *Calcrl*$^{fl/fl}$/*Prox1-CreER*^{T2} animals after either normal or HFD (Figure 1G,H). In addition, expression of key lipid transporters is dysregulated in *Calcrl*$^{fl/fl}$/*Prox1-CreER*^{T2} (Figure 1I). Together these data clearly indicate that lymphatic and enteroendocrine *Calcrl* is important for body fat mobilization and accumulation without affecting muscle mass or food and water consumption.

Livers Deficient in *Calcrl* Contain Reduced Lipids. The liver is a major site of metabolic homeostasis and governs the

DOI: 10.1021/acsptsci.8b00061
ACS Pharmacol. Transl. Sci. 2019, 2, 114−121

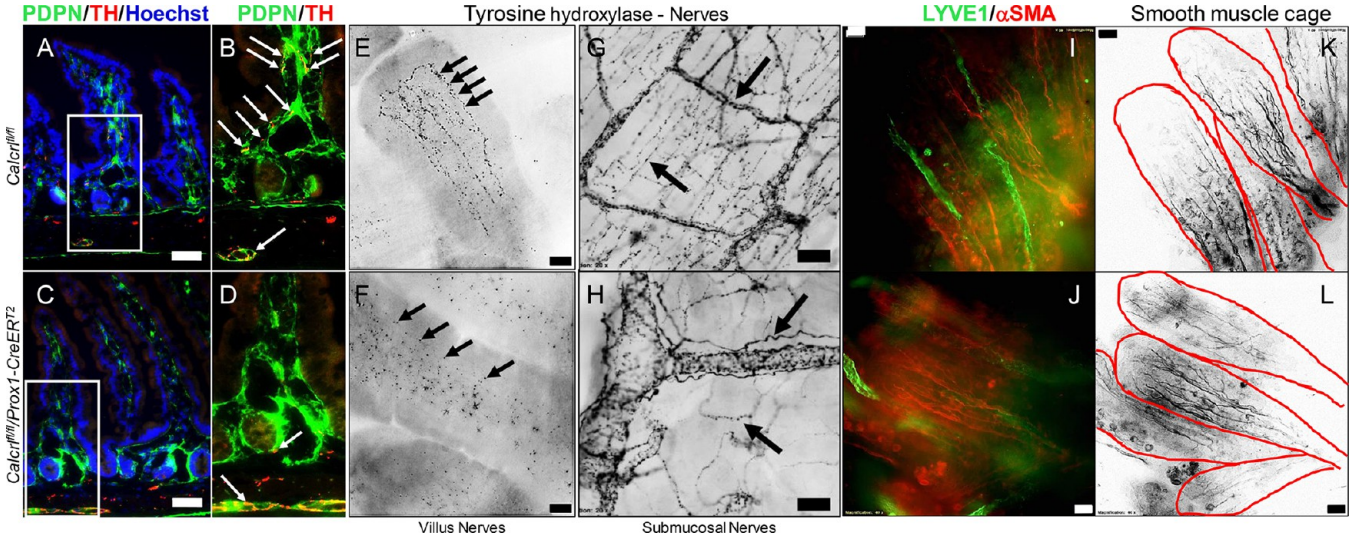

Figure 4. *Calcrl* governs enteric nerve density and organization but not the smooth muscle cage around intestinal villi. (A−D) Representative podoplanin/tyrosine hydroxylase/Hoechst stained sections of tamoxifen-treated $Calcrl^{fl/fl}$ and $Calcrl^{fl/fl}$/*Prox1-CreER*^{T2} animals after HFD challenge. Arrows highlight tyrosine hydroxylase-positive nerves along lymphatic endothelium. Boxed regions are displayed as digitally zoomed insets on the right of each image. (E, F) Representative tyrosine hydroxylase stained whole-mount duodenum from tamoxifen-treated $Calcrl^{fl/fl}$ and $Calcrl^{fl/fl}$/*Prox1-CreER*^{T2} animals after HFD challenge. Arrows highlight tyrosine hydroxylase-positive nerves within the villi. (G, H) Representative tyrosine hydroxylase stained whole-mount duodenum from tamoxifen-treated $Calcrl^{fl/fl}$ and $Calcrl^{fl/fl}$/*Prox1-CreER*^{T2} animals after HFD challenge. Arrows highlight tyrosine hydroxylase-positive nerves within the submucosa. (I−L) Representative LYVE1 and αSMA stained whole-mount intestinal villi of tamoxifen-treated $Calcrl^{fl/fl}$ and $Calcrl^{fl/fl}$/*Prox1-CreER*^{T2}. For all panels in Figure 4: $N = 6$ animals per genotype. Scale bars: 50 μm in (A-D); 20 μm in (E, F); 50 μm in (G, H).

storage and redistribution of lipids in coordination with intestines.[19] In addition, *Prox1* is expressed in liver hepatocytes.[20] We thus examined whether *Calcrl* depletion alters normal liver lymphatic vasculature, function, and lipid accumulation. $Calcrl^{fl/fl}$/*Prox1-CreER*^{T2} livers showed dilated LYVE1-stained vessels with decreased lipid accumulation (Figure 2A−F). Consistently, levels of fecal pancreatic lipase were increased in $Calcrl^{fl/fl}$/*Prox1-CreER*^{T2} without any histological changes in the pancreas themselves (Figure 2 G and data not shown). Blood glucose levels were downregulated in $Calcrl^{fl/fl}$/*Prox1-CreER*^{T2} animals (data not shown). Although triglyceride hydrolysis is controlled by lipoprotein lipase, the overall hepatic triglyceride production rate remained unchanged (Figure 2H). Collectively, these data indicate that the liver and pancreas play a limited role in *Calcrl*-driven body fat accumulation.

***Calcrl* Regulates Intestinal Lipid Trafficking.** We have previously published that lacteals of $Calcrl^{fl/fl}$/*Prox1-CreER*^{T2} mice were dilated, and consistently, submucosal lymphatics of these mice are also dilated (data not shown).[4] Intestinal lymphatics absorb and process dietary fat; therefore, to gain closer insights into the potential dysregulation of localized lipid uptake within the intestinal villus and lacteal, we characterized lipid trafficking and processing in tamoxifen-treated $Calcrl^{fl/fl}$ and $Calcrl^{fl/fl}$/*Prox1-CreER*^{T2} animals after both short- and long-term HFD challenge. Oil Red O staining of small intestine villi following a 2 week HFD challenge revealed robust accumulation of lipid throughout enterocytes and within the lumen of the lacteal in control mice (Figure 3A,B, black arrows and arrowhead). However, $Calcrl^{fl/fl}$/*Prox1-CreER*^{T2} mice showed no lipid within the lacteal and the enterocyte lipid deposits were predominantly localized to their apical border, suggesting abnormal chylomicron processing (Figure 3C,D, black arrows and arrowhead). Conventional staining to demarcate enterocyte borders, lymphatic endothelium, and villus blood vessels after BODIPY (fluorescent fatty acid) gavage further confirmed the mislocalization of lipids (Figure 3E−L). In the $Calcrl^{fl/fl}$/*Prox1-CreER*^{T2} villi the fatty acid dye failed to translocate to the basal side of the enterocytes and enter lacteals (Figure 3G,H,K,L). We did not observe any lipids within PECAM-labeled villi blood vessels (Figure 3J,L, asterisk). Importantly, control $Calcrl^{fl/fl}$ mice revealed LYVE1-positive lymphatic endothelium displaying prominent BODIPY accumulation between cells, indicative of the established paracellular transport route of lipids in lymphatics (Figure 3J, arrowhead). In contrast, the lacteal endothelium of $Calcrl^{fl/fl}$/*Prox1-CreER*^{T2} mice appeared thin, as previously described,[11] and contained abnormal accumulation of BODIPY within the cell bodies, suggestive of delayed transcellular import of lipid within LECs depleted of *Calcrl* (Figure 3L, arrowhead). Ultrastructural electron microscopy analysis of intestinal lacteals from HFD fed animals confirmed numerous defects in $Calcrl^{fl/fl}$/*Prox1-CreER*^{T2} mice compared to controls (Figure 3M−P) including: thin LECs with accumulation of foamy, lipid-laden cytoplasm, visibly stretched and electron "diffuse" LEC junctions (red brackets) and an expanded lacteal lumen with a paucity of proteinaceous lymph fluid (L) (Figure 3P, yellow arrowheads). Taken together, these results illustrate that spatiotemporal genetic deletion of *Calcrl* by the *Prox1-CreER*^{T2} driver leads to structural defects in lacteal LECs which impair the normal balance between paracellular and transcellular lipid transport governing the absorptive functions of intestinal lymphatics.

Loss of *Calcrl* Disrupts Lacteal and Submucosal Nerve Patterning. Lipid drainage through the lacteals is in part controlled by the enteric nervous system and the smooth muscle cage surrounding them.[9] Additionally, lacteals of larger animals have been shown to make direct contact with sensory nerve fibers that secrete CGRP, an alternative ligand interacting with *Calcrl*.[10] Therefore, we examined the smooth muscle cage layer and nervous patterning surrounding lacteals and submucosal

DOI: 10.1021/acsptsci.8b00061
ACS Pharmacol. Transl. Sci. 2019, 2, 114−121

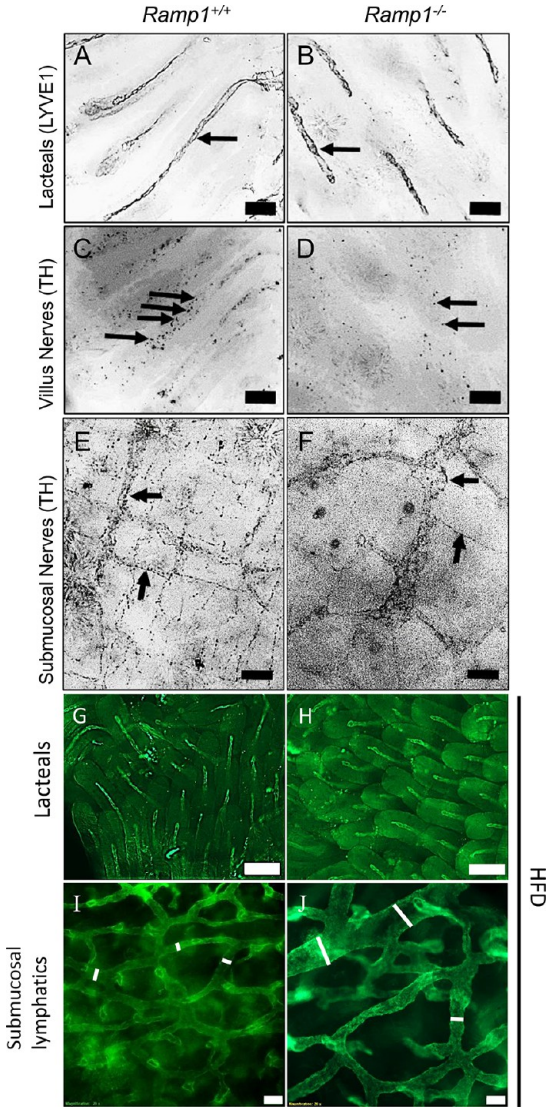

Figure 5. Reduced tyrosine-positive nerves in *Ramp1*$^{-/-}$ villi with disorganized submucosal nerves. (A–D) Representative tyrosine hydroxylase stained whole-mount duodenum of tamoxifen-treated *Calcrl*$^{fl/fl}$ and *Calcrl*$^{fl/fl}$/*Prox1-CreER*^{T2} animals after HFD challenge. Arrows highlight tyrosine hydroxylase-positive nerves within villi. (E, F) Representative tyrosine hydroxylase stained whole-mount duodenum from tamoxifen-treated *Calcrl*$^{fl/fl}$ and *Calcrl*$^{fl/fl}$/*Prox1-CreER*^{T2} animals after HFD challenge. Arrows highlight tyrosine hydroxylase-positive nerves within the submucosa. (G–J) Representative LYVE1 stained whole-mount intestinal lacteals and submucosal lymphatic capillaries of tamoxifen-treated *Calcrl*$^{fl/fl}$ and *Calcrl*$^{fl/fl}$/*Prox1-CreER*^{T2} animals after HFD challenge. For all panels in Figure 5: $N = 5$ *Ramp1*$^{+/+}$ and 3 *Ramp1*$^{-/-}$. Scale bars: 100 μm in (A, B); 50 μm in (C–J).

lymphatic vessels of tamoxifen-treated *Calcrl*$^{fl/fl}$/*Prox1-CreER*^{T2} mice after a HFD challenge. Importantly, *Calcrl*$^{fl/fl}$ lacteals demonstrated well-organized tyrosine hydroxylase-labeled nerve fibers while the nerves of *Calcrl*$^{fl/fl}$/*Prox1-CreER*^{T2} lacteals were reduced (Figure 4A–H). Furthermore, *Calcrl*$^{fl/fl}$ submucosa demonstrated densely packed nerves, while the nerves of *Calcrl*$^{fl/fl}$/*Prox1-CreER*^{T2} submucosal lymphatics were severely disorganized (Figure 4E–H). α-Smooth muscle actin (α-SMA) delineating the smooth muscle cage surrounding lacteals suggests no obvious role of *Calcrl* in smooth muscle patterning (Figure 4I–L). Collectively, these data highlight the requirement of *Calcrl* for enteric nervous patterning and suggest a role of the lack of adequate nervous control of lymphatic vessels in *Calcrl*$^{fl/fl}$/*Prox1-CreER*^{T2} in lipid absorption.

Global Depletion of RAMP1 Leads to Disorganization and Reduction in Enteric Nerve Density. The *Calcrl*-RAMP1 heterodimer forms the CGRP receptor, and this interface has recently been successfully targeted for the therapeutic treatment of migraine, indicating that the expression of RAMP1 determines whether and how a CLR-expressing cells will sense and respond to CGRP.[21−23] Therefore, to further substantiate the importance of *Calcrl* in governing enteric nervous patterning, we examined *Ramp1*$^{-/-}$ intestinal lymphatics and their associated nerves. *Ramp1*$^{-/-}$ animals display reduced density of tyrosine hydroxylase-labeled nerves surrounding the villus lacteals and disorganization of the submucosal nerves mimicking the results of *Calcrl*-depleted mice, in addition to presenting dilated lymphatic vessels (Figure 5A–F, as well as Figure 5G–J). Our results emphasize the importance of lymphatic and enteroendocrine *Calcrl*-RAMP1 signaling axis in autonomic nerve patterning.

DISCUSSION

In this study, we found that tamoxifen-inducible deletion of *Calcrl* in lymphatics resulted in reduced weight gain, coupled with dysregulated lipid trafficking and mispatterning of enteric nerves. Importantly, by utilizing *Prox1-CreER*^{T2} to delete floxed *Calcrl*, we were able to alter multiple systems that crosstalk in maintaining lipid homeostasis, previously studied in isolation. This study demonstrates that a lymphatic and enteroendocrine *Calcrl*/*Ramp1* axis balances the paracellular and transcellular pathways of lipid transport in addition to communicating with sensory nerves to govern lacteal drainage of lipids (Figure 6B,C).

Complete ablation of EECs in *Ngn3*-deficient mice impairs lipid absorption and results in severe diabetes and neonatal death.[12,24,25] Similar to EECs, the central lacteals of each intestinal villi make direct contact with sensory nerve fibers that secrete CGRP.[1,10] Additionally, hormones released from EECs into lymphatic fluid in response to nutrients in the gut can act on GPCRs of sensory afferent nerves communicating with lymphatic vessels.[1] Taken together, these studies imply a bidirectional communication wherein EECs release hormones into the lymph fluid, which are sensed by neurons to send messages to the brain, and the nerves secrete neuropeptides that communicate with the receptors on lymphatic vessels guiding their function (Figure 6C). Although both *Prox1* and *Calcrl* are expressed in intestinal LECs and EECs (Figure 6A),[4,26] these cells have minimal expression of *Ramp1*, which is used by *Calcrl* to bind CGRP. Therefore, the diminished nerve connections in *Calcrl*$^{fl/fl}$/*Prox1-CreER*^{T2} mice are likely due to reduced communication between lacteals and nerves themselves, thereby helping us distinguish the role of the lymphatic innervation in fat absorption, exclusive of EEC involvement.

CGRP is a neuropeptide ligand with wide distribution in the intestinal tract, where it directly interacts with lacteals. In one study, *CGRP*$^{-/-}$ male mice fail to gain weight compared to controls.[27] In contrast, other studies have demonstrated that losing CGRP increases food intake and that overexpressing RAMP1 results in increased activity with reduced weight gain.[28] An interesting aspect of our study is that global loss of *Ramp1* reduces the presence of villus nerves and results in disorganization of submucosal nerves (Figure 5). Taken together, these studies highlight the complex role of enteric CGRP/CLR/RAMP1 axis in lipid uptake and processing. Considering that

DOI: 10.1021/acsptsci.8b00061
ACS Pharmacol. Transl. Sci. 2019, 2, 114–121

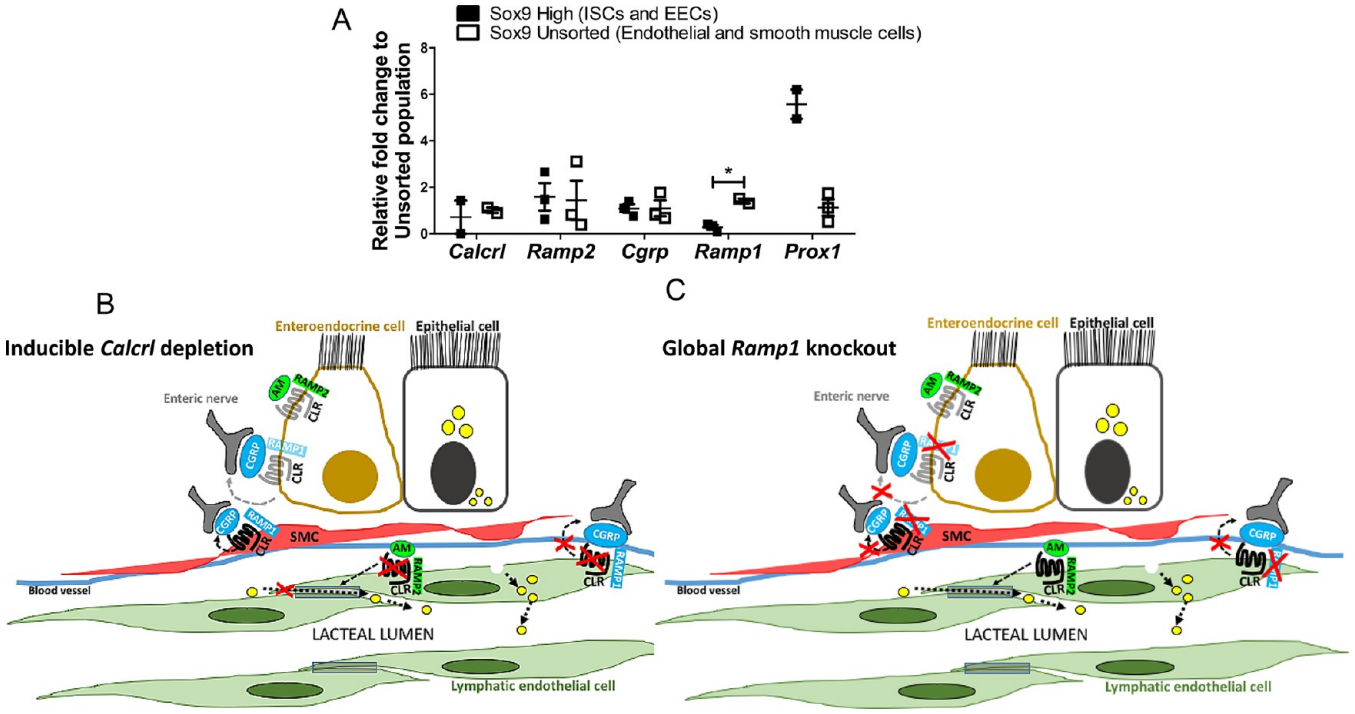

Figure 6. Loss of *Calcrl* from enteroendocrine cells and lymphatic endothelial cells. (A) Relative expression of receptors along the CLR signaling axis between Sox9 high and unsorted cells. Data are represented as mean ± SEM with significance determined by Student's *t* test: *, $P < 0.05$. $N = 3$ technical replicates. (B) Model representing deletion of *Calcrl* from the endothelial and enteroendocrine cells affecting endothelial junction and communication with enteric nerves. (C) Model depicting global loss of *Ramp1* prevents communication of smooth muscle cells (SMC), enteroendocrine cells (EECs), and lacteal endothelium with CGRP secreting enteric nerves.

several new drugs that directly inhibit the CGRP/CLR/RAMP1 axis have recently been approved for the clinical treatment of migraine,[21,23] it remains possible that gastrointestinal side effects may be related to the roles of this signaling pathway within the lacteal and enteroendocrine cell.

Defects in LEC junctions upon loss of CLR-AM signaling is perhaps expected, given previous studies by us and others demonstrating a key role for this pathway in tightening VE-Cadherin/ZO1 LEC complexes and mediating lymphatic permeability, both *in vitro* and *in vivo*.[4,6,29,30] However, we have a surprising lack of information regarding the potential downstream effector molecules of CLR-mediated LEC junction stabilization. Despite its importance in digestive function, we still do not fully understand the mechanisms through which lymphatic lacteals absorb chylomicrons and two opposing, but not mutually exclusive, theories about transcellular or paracellular transport pathways are debated.[31−34] This study suggests the role of linearized "zipper junctions" in reduced paracellular transport of lipids combined with an increase in vesicular transcellular transport ultimately leading to aberrant accumulation of lipid within lacteal LECs, which we attribute to the well-established role of AM peptide in lymphatics (Figure 6B).

In conclusion, by altering a GPCR that serves as the effector molecule for two different intestinal peptides, AM and CGRP, we have been able to correlate phenotypic changes in lipid absorption, enterocyte lipid trafficking, and neuronal communication within the intestine to the cell-specific functions of this receptor pathway in the neurolymphocrine unit (Figure 6B,C). The CLR signaling axis therefore represents a potential target for the therapeutic management of obesity and related intestinal disorders.

AUTHOR INFORMATION

Corresponding Author

*E-mail: Kathleen_Caron@med.unc.edu. Tel.: (919) 966-5215. Fax: (919) 843-1316.

ORCID

Kathleen M. Caron: 0000-0002-7033-9232

Author Contributions

R.B.D. and K.M.C.: study concept and design, analysis and interpretation of data, statistical analysidrafting of the manuscript, critical revision of the manuscript for important intellectual content, obtained funding, study supervision; R.B.D., S.D., N.R.N., J.B.P., and E.S.B.: acquisition of data.

Notes

The authors declare no competing financial interest.

ACKNOWLEDGMENTS

We are grateful to Drs. Martin J. Costello (Department of Cell Biology and Physiology, UNC−CH) and Hal Mekeel (Hooker Microscopy Imaging Core, UNC−CH) for their expertise in sample preparation and imaging consultation for TEM. We thank all members of the Caron lab for insightful discussion and technical support. Grant Support: NIH NIDDK099156, NIH NHLBI HL129086, AHA 16IRG27260077 to K.M.C.; AHA 15POST25270006 to R.B.D.

ABBREVIATIONS

GPCR, G protein coupled receptor; CGRP, calcitonin-gene-related peptide; RAMP, receptor activity modifying protein; CLR and *Calcrl*, calcitonin-receptor-like receptor

DOI: 10.1021/acsptsci.8b00061
ACS Pharmacol. Transl. Sci. 2019, 2, 114−121

REFERENCES

(1) Poole, D. P., Lee, M., Tso, P., Bunnett, N. W., Yo, S. J., Lieu, T., Shiu, A., Wang, J.-C., Nomura, D. K., and Aponte, G. W. (2014) Feeding-Dependent Activation of Enteric Cells and Sensory Neurons by Lymphatic Fluid: Evidence for a Neurolymphocrine System. *Am. J. Physiol. Liver Physiol. 306* (8), G686−G698.

(2) Nurmi, H., Saharinen, P., Zarkada, G., Zheng, W., Robciuc, M. R., and Alitalo, K. (2015) VEGF-C Is Required for Intestinal Lymphatic Vessel Maintenance and Lipid Absorption. *EMBO Mol. Med. 7* (11), 1418−1425.

(3) Bernier-Latmani, J., Cisarovsky, C., Demir, C. S., Bruand, M., Jaquet, M., Davanture, S., Ragusa, S., Siegert, S., Dormond, O., Benedito, R., et al. (2015) DLL4 Promotes Continuous Adult Intestinal Lacteal Regeneration and Dietary Fat Transport. *J. Clin. Invest. 125* (12), 4572−4586.

(4) Davis, R. B., Kechele, D. O., Blakeney, E. S., Pawlak, J. B., and Caron, K. M. (2017) Lymphatic Deletion of Calcitonin Receptor−like Receptor Exacerbates Intestinal Inflammation. *JCI Insight 2* (6), No. e92465.

(5) Baluk, P., Fuxe, J., Hashizume, H., Romano, T., Lashnits, E., Butz, S., Vestweber, D., Corada, M., Molendini, C., Dejana, E., et al. (2007) Functionally Specialized Junctions between Endothelial Cells of Lymphatic Vessels. *J. Exp. Med. 204* (10), 2349−2362.

(6) Triacca, V., Güç, E., Kilarski, W. W., Pisano, M., and Swartz, M. A. (2017) Transcellular Pathways in Lymphatic Endothelial Cells Regulate Changes in Solute Transport by Fluid StressNovelty and Significance. *Circ. Res. 120* (9), 1440−1452.

(7) Dunworth, W. P., Fritz-Six, K. L., and Caron, K. M. (2008) Adrenomedullin Stabilizes the Lymphatic Endothelial Barrier in Vitro and in Vivo. *Peptides 29* (12), 2243−2249.

(8) Gibbons, C., Dackor, R., Dunworth, W., Fritz-Six, K., and Caron, K. M. (2007) Receptor Activity-Modifying Proteins: RAMPing up Adrenomedullin Signaling. *Mol. Endocrinol. 21* (4), 783−796.

(9) Choe, K., Jang, J. Y., Park, I., Kim, Y., Ahn, S., Park, D. Y., Hong, Y. K., Alitalo, K., Koh, G. Y., and Kim, P. (2015) Intravital Imaging of Intestinal Lacteals Unveils Lipid Drainage through Contractility. *J. Clin. Invest. 125* (11), 4042−4052.

(10) ICHIKAWA, S., KASAHARA, D., IWANAGA, T., UCHINO, S., and FUJITA, T. (1991) Peptidergic Nerve Terminals Associated with the Central Lacteal Lymphatics in the Ileal Villi of Dogs. *Arch. Histol. Cytol. 54* (3), 311−320.

(11) Fritz-Six, K. L., Dunworth, W. P., Li, M., and Caron, K. M. (2008) Adrenomedullin Signaling Is Necessary for Murine Lymphatic Vascular Development. *J. Clin. Invest. 118* (1), 40−50.

(12) Mellitzer, G., Beucher, A., Lobstein, V., Michel, P., Robine, S., Kedinger, M., and Gradwohl, G. (2010) Loss of Enteroendocrine Cells in Mice Alters Lipid Absorption and Glucose Homeostasis and Impairs Postnatal Survival. *J. Clin. Invest. 120* (5), 1708−1721.

(13) Okano-Matsumoto, S., McRoberts, J. A., Taché, Y., and Adelson, D. W. (2011) Electrophysiological Evidence for Distinct Vagal Pathways Mediating CCK-Evoked Motor Effects in the Proximal *versus* Distal Stomach. *J. Physiol. 589* (2), 371−393.

(14) Bohórquez, D. V., Shahid, R. A., Erdmann, A., Kreger, A. M., Wang, Y., Calakos, N., Wang, F., and Liddle, R. A. (2015) Neuroepithelial Circuit Formed by Innervation of Sensory Enteroendocrine Cells. *J. Clin. Invest. 125* (2), 782−786.

(15) Li, M., Wetzel-Strong, S. E., Hua, X., Tilley, S. L., Oswald, E., Krummel, M. F., and Caron, K. M. (2014) Deficiency of RAMP1 Attenuates Antigen-Induced Airway Hyperresponsiveness in Mice. *PLoS One 9* (7), No. e102356.

(16) Millar, J. S., Cromley, D. A., McCoy, M. G., Rader, D. J., and Billheimer, J. T. (2005) Determining Hepatic Triglyceride Production in Mice: Comparison of Poloxamer 407 with Triton WR-1339. *J. Lipid Res. 46* (9), 2023−2028.

(17) Van Landeghem, L., Santoro, M. a., Krebs, a. E., Mah, a. T., Dehmer, J. J., Gracz, a. D., Scull, B. P., McNaughton, K., Magness, S. T., and Lund, P. K. (2012) Activation of Two Distinct Sox9-EGFP-Expressing Intestinal Stem Cell Populations during Crypt Regeneration after Irradiation. *AJP Gastrointest. Liver Physiol. 302*, G1111−G1132.

(18) Bernier-Latmani, J., and Petrova, T. V. (2016) High-Resolution 3D Analysis of Mouse Small-Intestinal Stroma. *Nat. Protoc. 11* (9), 1617−1629.

(19) Bechmann, L. P., Hannivoort, R. A., Gerken, G., Hotamisligil, G. S., Trauner, M., and Canbay, A. (2012) The Interaction of Hepatic Lipid and Glucose Metabolism in Liver Diseases. *J. Hepatol. 56* (4), 952−964.

(20) Dudas, J., Elmaouhoub, A., Mansuroglu, T., Batusic, D., Tron, K., Saile, B., Papoutsi, M., Pieler, T., Wilting, J., and Ramadori, G. (2006) Prospero-Related Homeobox 1 (Prox1) Is a Stable Hepatocyte Marker during Liver Development, Injury and Regeneration, and Is Absent from "Oval Cells. *Histochem. Cell Biol. 126* (5), 549−562.

(21) Silberstein, S. D., Dodick, D. W., Bigal, M. E., Yeung, P. P., Goadsby, P. J., Blankenbiller, T., Grozinski-Wolff, M., Yang, R., Ma, Y., and Aycardi, E. (2017) Fremanezumab for the Preventive Treatment of Chronic Migraine. *N. Engl. J. Med. 377* (22), 2113−2122.

(22) Hershey, A. D. (2017) CGRP — The Next Frontier for Migraine. *N. Engl. J. Med. 377* (22), 2190−2191.

(23) Goadsby, P. J., Reuter, U., Hallström, Y., Broessner, G., Bonner, J. H., Zhang, F., Sapra, S., Picard, H., Mikol, D. D., and Lenz, R. A. (2017) A Controlled Trial of Erenumab for Episodic Migraine. *N. Engl. J. Med. 377* (22), 2123−2132.

(24) Jenny, M., Uhl, C., Roche, C., Duluc, I., Guillermin, V., Guillemot, F., Jensen, J., Kedinger, M., and Gradwohl, G. (2002) Neurogenin3 Is Differentially Required for Endocrine Cell Fate Specification in the Intestinal and Gastric Epithelium. *EMBO J. 21* (23), 6338−6347.

(25) Gradwohl, G., Dierich, A., LeMeur, M., and Guillemot, F. (2000) Neurogenin3 Is Required for the Development of the Four Endocrine Cell Lineages of the Pancreas. *Proc. Natl. Acad. Sci. U. S. A. 97* (4), 1607−1611.

(26) Petrova, T. V., Nykänen, A., Norrmén, C., Ivanov, K. I., Andersson, L. C., Haglund, C., Puolakkainen, P., Wempe, F., von Melchner, H., Gradwohl, G., et al. (2008) Transcription Factor PROX1 Induces Colon Cancer Progression by Promoting the Transition from Benign to Highly Dysplastic Phenotype. *Cancer Cell 13* (5), 407−419.

(27) Liu, T., Kamiyoshi, A., Sakurai, T., Ichikawa-Shindo, Y., Kawate, H., Yang, L., Tanaka, M., Xian, X., Imai, A., Zhai, L., et al. (2017) Endogenous Calcitonin Gene-Related Peptide Regulates Lipid Metabolism and Energy Homeostasis in Male Mice. *Endocrinology 158* (5), 1194−1206.

(28) Muff, R., Born, W., Lutz, T. A., and Fischer, J. A. (2004) Biological Importance of the Peptides of the Calcitonin Family as Revealed by Disruption and Transfer of Corresponding Genes. *Peptides 25* (11), 2027−2038.

(29) Hoopes, S. L., Willcockson, H. H., and Caron, K. M. (2012) Characteristics of Multi-Organ Lymphangiectasia Resulting from Temporal Deletion of Calcitonin Receptor-Like Receptor in Adult Mice. *PLoS One 7* (9), e45261.

(30) Dunworth, W. P., and Caron, K. M. G. (2009) Protein-Coupled Receptors as Potential Drug Targets for Lymphangiogenesis and Lymphatic Vascular Diseases. *Arterioscler., Thromb., Vasc. Biol. 29* (5), 650−656.

(31) Dixon, J. B. (2010) Lymphatic Lipid Transport: Sewer or Subway? *Trends Endocrinol. Metab. 21* (8), 480−487.

(32) PALAY, S. L., and KARLIN, L. J. (1959) An Electron Microscopic Study of the Intestinal Villus. II. The Pathway of Fat Absorption. *J. Cell Biol. 5* (3), 373−384.

(33) Dobbins, W. O., and Rollins, E. L. (1970) Intestinal Mucosal Lymphatic Permeability: An Electron Microscopic Study of Endothelial Vesicles and Cell Junctions. *J. Ultrastruct. Res. 33* (1), 29−59.

(34) Azzali, G. (1982) The Ultrastructural Basis of Lipid Transport in the Absorbing Lymphatic Vessel. *J. Submicrosc. Cytol. 14* (1), 45−54.

DOI: 10.1021/acsptsci.8b00061
ACS Pharmacol. Transl. Sci. 2019, 2, 114−121